

The effect of observed vertical structure, habits, and size distributions on the solar radiative properties and cloud evolution of cirrus clouds

Huiyi Yang,^{a,b,c,*} Steven Dobbie,^b Ross Herbert,^b Paul Connolly,^d Martin Gallagher,^d Sat Ghosh,^e Sardar M. R. K. Al-Jumur^b and James Clayton^b

^a*CMA Key Laboratory for Atmospheric Physics and Environment, Nanjing University of Information Science and Technology, China*

^b*Institute for Climate and Atmospheric Science, School of Earth and Environment, University of Leeds, UK*

^c*AOPP, Department of Physics, University of Oxford, UK*

^d*School of Earth, atmospheric and environmental Sciences, University of Manchester, UK*

^e*School of Mechanical and Building Sciences, Vellore Institute of Technology, Tamil Nadu, India*

*Correspondence to: H. Yang, AOPP, Department of Physics, University of Oxford, Oxford OX1 3PU, UK.
E-mail: huiyi.yang@physics.ox.ac.uk

Cirrus observations taken during EMERALD1 clearly showed vertical structure in ice crystal habit and size distribution. In this study, we use these observations along with radiative and cloud modelling to assess the importance of this observed vertical structure in size and habit on radiative properties and cloud evolution. We show that neglecting the vertical structure results in changes to the solar upwelling and downwelling fluxes of 10 and 8 W m⁻², respectively. If further simplifications are made and aggregate and rosettes are treated more simplistically (as columns) then the upwelling and downwelling fluxes are altered by about 16 and 12 W m⁻², respectively. It was noted that the effects of simplifying the vertical structure and habits act in competing ways in terms of the fluxes and therefore emphasize the need to consider both effects in order to improve modelling rather than considering either in isolation.

Often, general circulation models have highly parametrized treatments of cloud properties. We illustrate that crude assumptions about ice crystal effective sizes used in models (from the literature) can result in fluxes being in error by 100 W m⁻² or more compared to using the observations. The above results are contrasted with effects of ice crystal roughness (altering the asymmetry). We show that moderate estimates of roughness lead to changes in the upward and downward fluxes of about 10–15 W m⁻². This shows that vertical structure, habits and knowledge of size distribution are key factors and on a par with such effects as ice particle roughness, which is considered to have a highly uncertain but important cirrus radiative effect.
Copyright © 2011 Royal Meteorological Society

Key Words: cirrus; ice crystals; habits, radiative properties; EMERALD; vertical structure; ice optics

Received 19 April 2011; Revised 2 September 2011; Accepted 17 October 2011; Published online in Wiley Online Library

Citation: Yang H, Dobbie S, Herbert R, Connolly P, Gallagher M, Ghosh S, Al-Jumur SMRK, Clayton J. 2011. The effect of observed vertical structure, habits, and size distributions on the solar radiative properties and cloud evolution of cirrus clouds. *Q. J. R. Meteorol. Soc.* DOI:10.1002/qj.973

1. Introduction

Cirrus clouds have been identified as one of the most important unsolved issues in the radiation budget of the Earth–atmosphere system (Liou, 1986; Dowling and Radke, 1990; Zhang and Mace, 2006). The coverage of cirrus clouds is about 30% on a global average at any given time (Wylie and Menzel, 1999), up to 60–70% in the Tropics (Wylie *et al.*, 1994; Baran, 2009), and even higher if the sub-visible ice clouds with optical thickness (τ) less than 0.03 (Wang *et al.*, 1996) are included. Cirrus can occur in a wide vertical range extending to the upper troposphere and lower stratosphere in the Tropics and mid-latitudes, and lower troposphere in the polar regions during winter (Key *et al.*, 2002).

The influence of cirrus clouds depends strongly on their radiative properties. The net radiative effect on shortwave and thermal radiation is still not fully resolved (Lindzen *et al.*, 2001; Lin *et al.*, 2002; Fu *et al.*, 2002), but the effect of cirrus on the radiation balance depends strongly on the coverage of thin relative to thick cirrus cloud (Chou *et al.*, 2002) and generally has a net warming effect.

Cirrus clouds are dominated by complex non-spherical ice particles that range widely over size and shape (Heymsfield and Platt, 1984; Heymsfield and McFarquhar, 2002). The uncertainty of radiative forcing and cloud feedback is understood to be mainly due to the optical properties of ice particles, which are most frequently represented in numerical models by extinction coefficient, single-scatter albedo (SSA) and asymmetry factor. Given that ice particles in cirrus are comparable or larger than solar wavelengths, the optical properties are often dependent on ice particle details such as particle size distribution, particle shape, surface roughness and concavity. Ice particles have been observed to vary in shape from individual columns to quite complex shapes, such as irregular or aggregate (Field and Heymsfield, 2003; Baran and Labonnote, 2007; Um and McFarquhar, 2009). Particle sizes range from a few micrometres in high tropical cirrus (McFarquhar and Heymsfield, 1996) to several hundred micrometres in mid-latitude frontal cirrus (Heymsfield and Miller, 1990; Wang and Sassen, 2001).

The first widely used treatment of ice crystal optics was by Ebert and Curry (1992), which made the assumption of equivalent spheres. This was greatly improved upon by the use of the geometric ray tracing method by Takano and Liou (1989), which assumed that particles were of hexagonal shape. This has been improved upon over the years by Takano and Liou (1995) and Macke (1993) and extended to more complex shapes including irregulars and rosettes (e.g. Yang *et al.*, 2000; McFarquhar *et al.*, 2002; Fu, 2007). Key *et al.* (2002) showed that various habits can lead to a significant difference in upwelling and downwelling fluxes, and the work by Kahnert *et al.* (2007) shows using a general circulation model (GCM) that including non-spherical shape is equally important with ice particle number density or particle mass. Ice crystal optical properties have been developed as functions of effective size for simplicity of use in cloud resolving, regional and global models (e.g. Ebert and Curry, 1992; Fu, 1996; McFarquhar *et al.*, 2002; Edwards *et al.*, 2007). Climate and numerical weather prediction (NWP) models used in forecasting do not have the benefit of knowing ice crystal habit or vertical properties. This paper helps to illustrate the potential downside of ignoring these effects.

Some past work has been done investigating habit and vertical structure. Use of ice crystal particle shape (Lemke *et al.*, 1999) and vertical distribution (Gu and Liou, 2004) from First International Satellite Cloud Climatology Project (ISCCP) satellite observations in a GCM has shown a strong influence on the radiative properties. Yang *et al.* (2001) considered the case of a three-layer cirrus cloud based on the ISCCP Regional Experiment (FIREII) to investigate the bidirectional reflectance of vertical inhomogeneity relevant to the Moderate-Resolution Imaging Spectroradiometer (MODIS) satellite retrievals. In terms of modelling, Liu *et al.* (2003) investigated the effects of changing modelled clouds from one habit type to another, cycling through columns, rosettes, plates, and then spheres. Their work illustrated a significant sensitivity of the cloud evolution of ice water content, mean size, and radiative heating rates to the changes.

The work of Liu *et al.* (2003) provides useful bounds on the impact of habit on cirrus cloud since they took the approach of switching the whole cloud between different habit types, but these are extreme ‘bounding’ cases, and also no account was made of the vertical structure. Their results for cloud evolution indicate significant effects that we want to test this under with observed, albeit case-specific, conditions. In our approach, we have taken a similar line to Yang *et al.* (2001) in that we utilize *in situ* aircraft observations of vertical structure for habits and size distributions and couple this with rigorous case-specific optics calculations to evaluate the cloud and radiative properties. Our work focuses on the radiative fluxes rather than the bidirectional reflectances which appeal to satellite retrieval. In addition, we include cloud modelling to assess the effects of vertical structure and habit on cloud evolution, building on the work of Dobbie and Jonas (2001), and their relative importance. Finally, this work takes the approach of assessing what uncertainty is introduced by using less and less observed complexity in habit and vertical structure and observed knowledge in general. This sensitivity and the impact on the top of the atmosphere and surface fluxes are instructive for large-scale modellers introducing updates to their models such as more detailed habit specifications.

2. Case study

We have selected the EMERALD1 observations on which to base this study since the crystal habit and size distribution have already been analysed for certain flights; one in particular has straight and level flights through the cloud at four heights that show distinct ice particle regions in the cloud.

The Egret Microphysics with Extended Radiation and Lidar (EMERALD) campaign designed to study dynamics, microphysics and radiation. EMERALD1 was conducted from Adelaide, Australia, during September 2001 and focused on the properties of mid-latitude frontal cirrus. EMERALD2 was conducted at Darwin, Australia, during November 2002 and focused on the cirrus anvil outflow originating from deep convection. There were ten scientific flights in each project, detailing the cloud and surrounding air.

The results of the EMERALD1 campaign were summarized in papers describing the cloud and microphysical structure of the cloud (Whiteway *et al.*, 2004; Gallagher *et al.*, 2005). A series of flights at various levels within the

cloud allowed for an assessment of the vertical structure in terms of size distribution and habit.

For this research, we focused on the ninth flight of EMERALD1 (labelled EM09). The EM09 flight was on 19 September 2001, and two aircraft were involved: a Super King Air B200T and a Grob Egret T520, which was instrumented from Airborne Research Australia. The Super King Air flew below the clouds at about 7 km altitude with an upward viewing laser–radar (lidar). The Egret flew within the cloud at a higher altitude, making measurements of the microphysical properties of cloud, such as cloud size distribution, humidity, turbulence, ozone, and pictures of the ice crystal habit. A great benefit of the Egret is that it can fly slowly at high altitude (80–100 m s⁻¹) owing to a long wingspan, so this enabled the Super King Air and the Egret to fly in a stacked formation approximately 1–2 km between each other, on average.

During the EM09 flight, the Egret flew through the cloud at four distinct levels to sample the vertical structure of cloud in terms of the size distribution and ice particle habit. The observations show that the range of cloud top of EM09 is between 9 and 12 km and the cloud base is between 7 and 8.5 km. The averaged ice number concentration is 693 L⁻¹, the maximum ice number concentration is 4176 L⁻¹, the mean particle size is 64 µm, and the maximum particle size is 769 µm, as determined from the Cloud Particle Imaging (CPI) instrument (Gallagher *et al.*, 2005). The mean particle size is an average of all the ice particles for each flight. For full details, including lidar images of the cloud and images of the observed ice crystals, see Gallagher *et al.* (2005).

Ice crystal habit has been evaluated from the CPI and have been processed for the four layers, labelled (a), (b), (c) and (d), with (a) at the top of the cloud and (d) at the base. Habit was categorized into various types for each layer: spheroids budding rosette, large rosette, column, plate, small irregular and large irregular. Figure 1 shows the habit-segregated size distributions of layers (a), (b), (c) and (d). The Forward Scattering Spectrometer Probe (FSSP, model DMT SPP-100) spectra are also shown in the plots, except for run (c), when it failed. We do not expect particle shattering to be a significant factor in our results. We base this on good agreement between CPI and FSSP concentrations at the overlap region. Also, by analysing the arrival times of ice crystals measured by the CPI with statistics shown in Figure 2, it is clear that almost all images have only one particle present, but few have two and even fewer have three particles. We can compare this to a Poisson distribution to assess the randomness of the particle arrivals. If randomness is observed then it points to shattering not being important, as shattering would produce some bias in arrival times. The parameter for the Poisson distribution was calculated from the mean number of particles per image. We determined that the mean number of particles per image is 0.035 (which is the lambda parameter for the Poisson distribution) (Connolly *et al.*, 2007). Plotting a Poisson distribution on top of the CPI histogram reveals that they are almost the same. Included in the plot is a curve for Lambda = 0.70 just to illustrate how sensitive the result is to a doubled ice concentration. These results indicate that there could only be a very small amount of shattering occurring, since the number of frames with three particles in it (orders of magnitude less than frames with one or two particles) is only slightly more than that expected by randomness.

Bullet rosettes were observed at the top of the cloud and grew slightly and sedimented. They also fragmented into columns, and so at lower altitudes in the cloud there were far fewer rosettes left, but a greater abundance of columns and budding rosettes. For a detailed assessment of the cloud, further details concerning the EMERALD project can be found in Whiteway *et al.* (2004) and Gallagher *et al.* (2005).

3. Research tools

Two key research tools that are used in this study are the Fu–Liou radiation scheme (Fu and Liou, 1992, 1993; Fu *et al.*, 1998; Marsham and Dobbie, 2005), to quantitatively assess the importance of the vertical structure (size distribution and habit vertical variation) on the radiative properties, and the Large Eddy Model (LEM), to simulate the cirrus cloud evolution. These tools are now described.

3.1. Large Eddy Model and initialization

The base version LEM 2.3 (Mason, 1989; Gray *et al.*, 2001) is used in this study to model the cirrus cloud (Dobbie and Jonas, 2001; Marsham and Dobbie, 2005; Marsham *et al.*, 2006) in order to provide time-evolving profiles of cirrus and to assess the potential importance of vertical structure effects on the cirrus cloud evolution. Our LEM simulations are intended to be representative of case EM09 rather than a comprehensive case study. Ice water content profiles were not available from the EMERALD1 observations, so we use the LEM to provide a representative case.

The LEM code we used includes a fully coupled Fu–Liou radiation scheme to address the radiative properties of ice crystals. Details of the radiation scheme are provided below and in papers such as Dobbie and Jonas (2001), Marsham and Dobbie (2005) and Marsham *et al.* (2006). The LEM performs numerical integrations using basic equations for momentum, thermodynamics and continuity. The model is non-hydrostatic; use is made of the deep anelastic approximation (quasi-Boussinesq), which allows for small pressure and density deviations from a reference hydrostatic state (with sound waves filtered). The boundary conditions are periodic in the horizontal and the top and surface boundary conditions are rigid lids.

The simulations were run in 3D model domain, which was 20 km in the vertical and 5 × 5 km in the horizontal. The horizontal resolution is 100 m and the vertical resolution varies with height but maintains a resolution of 125 m in the layers in and around cloud, e.g. between 4.5 and 12.5 km. The LEM was initialized with a sounding taken from the Australian Bureau of Meteorology for Adelaide at 1116 UTC (Figure 3). A 2 h spin-up was more than sufficient to allow for realistic turbulence to establish (Dobbie and Jonas, 2001; Marsham and Dobbie, 2005; Marsham *et al.*, 2006). The total model simulation time was 4 h. For the first half hour of spin-up time, the forcing was steadily increased to a constant value at half an hour, which is then applied as constant until 2 h and then the forcing is shut off and the cloud decays. The forcing is only applied in the region of the cloud and is linearly decreased to zero above and below the cloud layer (at 1 and 15 km). We use ±10% water vapour and ±0.1 K temperature perturbations applied in the first time step to initialize structure in the atmosphere throughout the domain.

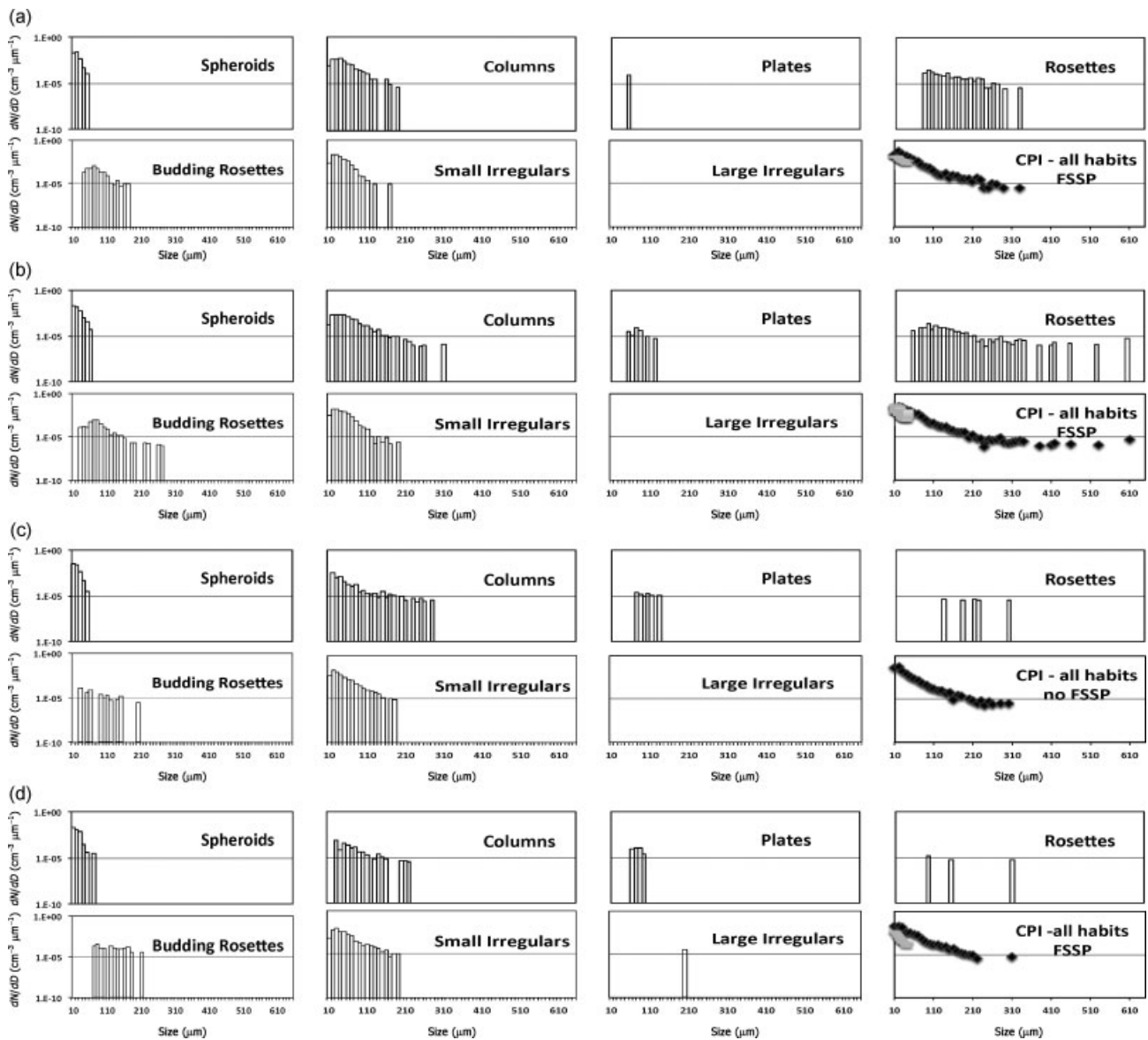


Figure 1. EMERALD1 EM09 habit segregated size distributions, dN/dD , from the CPI and FSSP observations for each layer. The top eight plots are for layer (a), the next eight are for layer (b), then layer (c) and layer (d).

The ice water path (IWP) varies during the simulation according to LEM evolution initialized with the EMERALD1 sounding. Figure 4 shows a profile of ice number concentration after 120 min of simulation time and comparison with EM09 average concentration. A time of 165 min is also used in this study since it is when our model IWC agrees with the observed average IWC EM09 for the flight segments involved in the vertical structure observations. The vertical structure in size distribution and habit is taken from the EMERALD1 observations, which are averaged values for the flights, and these are imposed throughout the simulation. This vertical structure in habit and size distribution is used in the radiation scheme to determine the radiative properties in conjunction with the time-evolving ice water path from the LEM.

3.2. Radiation model

The radiation model used is by Fu and Liou (1992, 1993) with the ice radiation package (Fu, 1996; Fu *et al.*, 1998) and is coupled with LEM for testing the radiative properties,

as was done for Dobbie and Jonas (2001), Marsham and Dobbie (2005), Marsham *et al.* (2006), and Yang (2009). The radiative transfer equation is solved using a discrete-ordinate δ four-stream solution approach; the details are discussed in books such as Liou (1986) or papers such as Li and Dobbie (1997).

The δ four-stream solution is a 1D solution which is applied to all columns in the LEM independently. The Fu–Liou radiation model uses six solar and 12 infrared bands. The radiation scheme is linked in the LEM to ice, liquid droplets, rain, graupel, snow, etc., and computes the scattering (Rayleigh) and absorption by gases.

The correlated k -distribution method is used to treat the gaseous absorption by O_3 , CO_2 , CH_4 , N_2O and H_2O . The CO_2 , CH_4 and N_2O are assumed to have uniform mixing ratios throughout the atmosphere, with concentrations of 330, 1.6 and 0.28 ppmv, respectively. A standard atmosphere mid-latitude autumn vertical profile is used for the gases. For the radiative transfer calculations, the inhomogeneous atmosphere is divided into n adjacent homogeneous vertical layers in which the single-scattering properties are constant

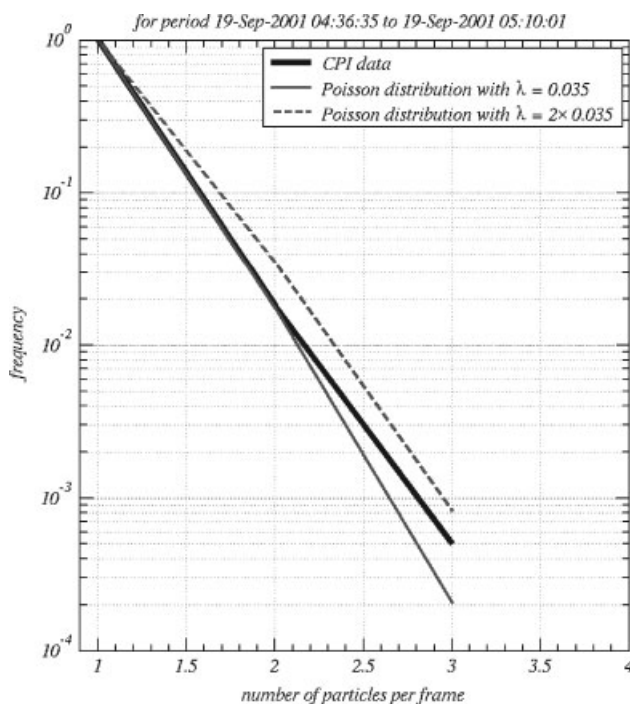


Figure 2. Frequency distribution of CPI arrival times *versus* the Poisson distribution of random arrival times for observed ice concentration and double observed ice concentration.

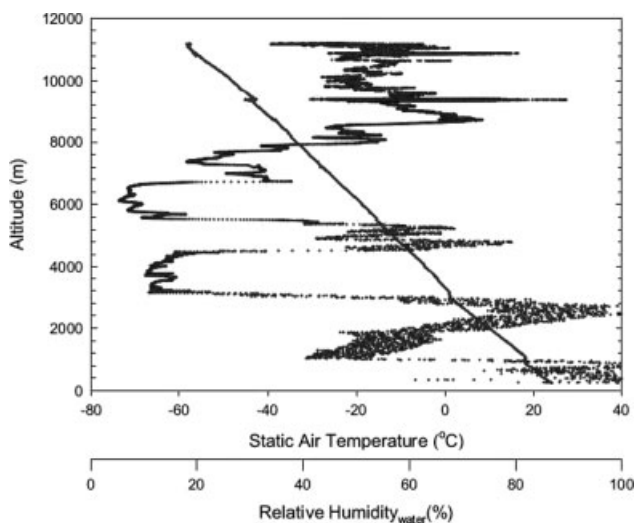


Figure 3. Initial sounding (static air temperature and relative humidity) for the EMERALD1 case (Gallagher *et al.*, 2005).

within each layer but vary between layers. The δ four-stream is employed to solve the radiative properties, applying continuity conditions at layer interfaces and standard boundary conditions. For the LEM, radiation is solved in this way for each column independently, commonly known as ‘independent pixel approximation’. Radiative properties are obtained for each of the spectral bands, with the solar spectral irradiance determined by Thekaekara (1973) and total solar flux of 1340 W m^{-2} . The solar zenith angle is set to 60° , the surface albedo to 20% and the emissivity of the surface to 1.

For cloud ice particles, the often-used method to specify the optical properties is in terms of the effective size (D_e) (for water clouds; see Dobbie *et al.*, 1999) or generalized effective size D_{ge} (Fu, 1996), and typical values used in models are between 20 and $120 \mu\text{m}$ (Fu, 1996).

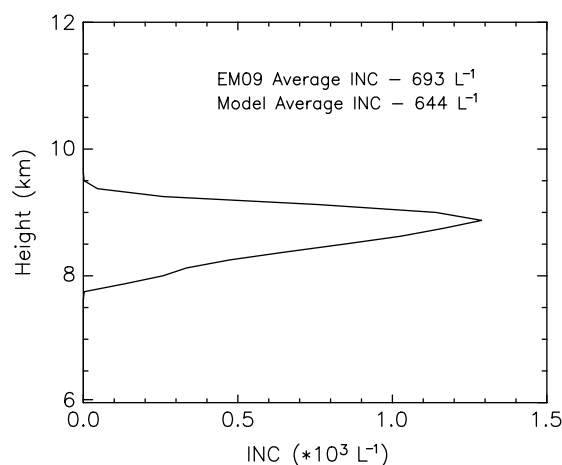


Figure 4. The plot shows ice number concentration at 120 min into the simulation. The average ice number concentration is inset and agrees with the observed value almost exactly at 693 L^{-1} .

4. Methodology

We focus especially on isolating various factors pertaining to the vertical structure and ice particle properties of cirrus in this work. By utilizing the research tools of the LEM and the Fu–Liou radiation scheme in conjunction with the EMERALD1 EM09 observations of the habit and size distributions for the four distinct vertical layers, we are able to assess the importance of observed habits and size distributions to progressively more simplified cases on the radiative properties of a representative cirrus cloud and its time evolution.

To achieve this, we have devised several cases with different assumptions to isolate effects. The cases range from assuming no knowledge of the cirrus layer and hence using standard, commonly used generalized effective sizes in the Fu–Liou scheme, progressing through to the most complex case of utilizing the vertical specification of habit and size distributions from EMERALD1 EM09 to calculate the radiative properties specific for the EMERALD1 EM09 case.

To compute the optical properties for the various habits, we have selected the optics compilation by Baran and Yang (compilation provided upon request from Dr Anthony Baran, UK Met Office). The database has been constructed from numerical simulations of individual crystals by a combination of methods as described in Baran and Francis (2004). [Correction added on 22 December 2011 after original online publication: in the preceding two sentences some text and citations have been replaced with the citation of Baran and Francis, 2004.] EMERALD1-specific optical properties are calculated by direct integrations of the single-scattering optical properties over the size distributions for each habit for each vertical layer from the observations weighted by solar flux in a similar way to Dobbie *et al.* (1999), as described later.

We now describe the cases that have been devised to isolate the different effects of vertical structure, size distributions, and habits with increasing simplification.

4.1. Base runs

Several base runs have been devised to test the radiative and evolution effects of cloud vertical structure in size

distribution and habit with, as mentioned, assumptions ranging from the most complex to the most simplistic. The cases are described below.

In order to use the observed size distribution as well as habit, we need to resort to calculating the optical properties from single-particle optics. In the optics compilation by Baran and Yang the shapes of columns and aggregates are available for individual modelled crystals at specific wavelengths. We therefore devise the following cases. Case 1 is the most detailed case, with optics derived from the Baran and Yang compilation for the four levels using habit information and size distribution for derivation of the optical properties. In this case, column single-scattering properties are used to approximate the EM09 columns, plates and small spheroids (which may indeed be small columns) and aggregate single-scattering properties are used to approximate the EM09 aggregates and rosettes. In case 2, we treat all crystals as columns, which is a commonly used assumption. This allows us to isolate the effects of rosette and aggregate crystal shapes by comparing cases 1 and 2. In case 3, we homogenize the vertical and use only columns to compute the optical properties. This allows assessment of simplifying one more step in terms of the vertical structure. For cases 4–7 we use the Fu–Liou hexagonal column approximation with the typical range of observed generalized effective size from 20 to 120 μm (Fu, 1996; Baran *et al.*, 2001; Stubenrauch *et al.*, 2007). These cases show the effect of using a wide range in commonly observed generalized effective sizes and allows us to determine the effect of little or no knowledge of cloud observations compared to our fullest knowledge of cloud properties (case 1).

Case 5 is a special one in that this is the generalized effective size (37.4 μm) was derived from the size distributions for EMERALD1 EM09.

- Case 1 is labelled the COLAGG run and uses the columns and aggregates of Baran’s compilation. The vertical variations in size distribution and habit used are taken from EMERALD1 observations.
- Case 2 is labelled the COL run. In this run, we use only Baran’s compilation of columns for all habits. The vertical variation of size distributions and habits used are taken from EMERALD1 observations.
- Case 3 is labelled COLHOMO. This run uses Baran’s compilation of columns for all habits and averages the results in the vertical, so there is no vertical variation inside the cloud.
- Case 4 is labelled COL20. This run uses the standard Fu–Liou model of optical properties with a fixed generalized effective size of 20 μm .
- Case 5 is labelled COL37. This is the same as case 4 but with a generalized effective size of 37 μm . This value was chosen based on calculating the value from the EMERALD1 size distributions.
- Case 6 is labelled COL80. This is the same as case 4 but with a fixed generalized effective size of 80 μm .
- Case 7 is labelled COL120. This is the same as case 4 but with a fixed generalized effective size of 120 μm .

4.2. Calculation of optical properties from the EMERALD1 observations

The Fu–Liou radiation scheme requires the extinction and scattering coefficients, SSA, and four moments of the phase

function including the asymmetry. From the Egret aircraft observations, we have the maximum projected length (D_p), which we take to be the maximum length of the crystal L and the size distribution ($n(L)$) for each habit. For columns, the particle diameter (D) (Mitchell and Arnott, 1994) is calculated by

$$\begin{aligned} D &= 0.7 \times L & L < 100 \mu\text{m} \\ D &= 0.0696 \times L^{\frac{1}{2}} & L \geq 100 \mu\text{m}. \end{aligned} \quad (1)$$

The volume of ice particle ($V(L)$) (Auer and Veal, 1970; Mitchell and Arnott, 1994) is

$$\begin{aligned} V(L) &= 0.1823 \times L^{2.908} & L < 100 \mu\text{m} \\ V(L) &= 0.0018 \times L^{1.908} & L \geq 100 \mu\text{m}. \end{aligned} \quad (2)$$

The projected area ($P(L)$) (Auer and Veal, 1970; Mitchell and Arnott, 1994) is

$$\begin{aligned} P(L) &= 0.1591 \times D^2 + 0.525 \times D^2 & L < 100 \mu\text{m} \\ P(L) &= 0.0016 \times D + 0.0522 \times D^{1.5} & L \geq 100 \mu\text{m}. \end{aligned} \quad (3)$$

For the rosettes, we use the approach of Mitchell and Arnott (1994) using a six-branched rosette model, which agrees with EMERALD CPI images. For irregular ice crystals, we follow the approach of Baran and Labonnote (2007) using the five-column irregular structure from the ensemble model, as the EMERALD observations indicated that almost exclusively small irregulars were present.

The ice water content (IWC) (Baran and Labonnote, 2007) is defined as

$$\text{IWC} = \rho \int V(L)n(L)dL, \quad (4)$$

where ρ is density of ice, which is assumed to be 0.92 g cm^{-3} (Baran and Labonnote, 2007), and $V(L)$ is the geometric volume of the ice crystals. The extinction/scattering coefficient is given by

$$\beta_{\text{ext/sca}} = \int Q_{\text{ext/sca}}(L)P(L)n(L)dL, \quad (5)$$

where $Q_{\text{ext/sca}}(L)$ is the extinction/scattering efficiency factor and $P(L)$ is the orientation-averaged projected area for a single crystal. The SSA (Fu and Liou, 1992), w_0 , is given by

$$w_0 = \frac{\int \omega^*(L)\beta_{\text{ext}}(L)n(L)dL}{\int \beta_{\text{ext}}(L)n(L)dL}, \quad (6)$$

where ω^* is the size-dependent SSA of individual ice particles (Fu and Liou, 1992). The asymmetry factor, g , is given by

$$g = \frac{\int g^*(L)\omega^*(L)Q_{\text{ext}}(L)n(L)dL}{\int \omega^*(L)Q_{\text{ext}}(L)n(L)dL}, \quad (7)$$

where g^* is the asymmetry factor, which is size dependent (Fu and Liou, 1992). In terms of Legendre polynomials P_n , the phase function P (Liou, 2002) is given by

$$P(\cos \theta) = \sum_{n=0}^N \omega_n P_n(\cos \theta), \quad (8)$$

where θ is the scattering angle and w_n are the expansion coefficients, given by

$$\omega_n = \frac{\int \omega_n^*(L)\omega^*(L)Q_{\text{ext}}(L)n(L)dL}{\int \omega^*(L)Q_{\text{ext}}(L)n(L)dL} \quad (n = 0, 1, 2, 3, 4), \quad (9)$$

where ω_n^* is the size-dependent expansion coefficient. All of the equations above were evaluated at individual wavelengths. To obtain the band-averaged results these were averaged with weighting from the incident solar spectrum (Thekaekara, 1973) at each wavelength within each band (Dobbie *et al.*, 1999; Liou, 2002):

$$\beta_{\text{band-avg}} = \frac{\int \beta_{\text{ext}}si \, d\lambda}{\int si \, d\lambda}. \quad (10)$$

The band-averaged SSA is

$$\omega_{0 \text{ band-avg}} = \frac{\int \omega \beta_{\text{ext}}si \, d\lambda}{\int \beta_{\text{ext}}si \, d\lambda}. \quad (11)$$

The band-averaged asymmetry factor is given by

$$g_{\text{band-avg}} = \frac{\int g\omega \beta_{\text{ext}}si \, d\lambda}{\int \omega \beta_{\text{ext}}si \, d\lambda}. \quad (12)$$

The band-averaged weighting functions for the Legendre polynomials are given by

$$\omega_n \text{ band-avg} = \frac{\int \omega_n \omega \beta_{\text{ext}}si \, d\lambda}{\int \omega \beta_{\text{ext}}si \, d\lambda}, \quad (13)$$

where si is the spectral solar irradiance and integrations are over wavelength ranges appropriate for each band in the Fu–Liou band structure.

EMERALD1-specific optical properties were computed from the observed habit and size distributions using the Baran and Yang compilation, which included 24 sizes and 56 wavelengths and were averaged into the band structure (see Fu, 1996). The resulting single-scattering optical properties included extinction and SSA, and the four moments (including the asymmetry factor) of the scattering phase function were then installed in the Fu–Liou radiation scheme in the LEM.

Figure 5 shows the results of optical properties for the seven base cases for the solar bands that range from 0.2 to 4.0 μm in wavelength. The left-hand column indicates the extinction normalized by the IWC, and SSA and asymmetry factor (g) for four layers and for column habit only from top to bottom. The middle column indicates column and aggregate habit, which is the most accurate representation of the optics. The right-hand column illustrates the optical properties using the typical approach of specifying an assumed effective radius with no vertical structure. The COLHOMO treatment of the optical properties is the same as COL except that the four layers of optical properties are averaged into one homogenized layer.

The first row in Figure 5 for the extinction normalized by the IWC shows that generally the two upper vertical layers are more similar than the two lower layers in the EMERALD1 EM09 observations. The different vertical layers

inside the cirrus cloud show significant differences in optical properties, which increases by a factor of almost two from the upper to the lower layers for both COLAGG and COL cases. COL80 and COL120 are significantly lower than all the others by as much as a factor of almost ten when comparing COLHOMO to COL120. The values of generalized effective size of 80 μm (COL80 case) and 120 μm (COL120 case) are far larger than the observational derived effective size, which is 37 μm . The COLHOMO is a simple average of the optical properties in column 1 of Figure 5.

The second row in Figure 5 shows the SSA. In all of the SSA plots it is clear that there is strong absorption in the near-infrared bands, especially in bands 5 and 6. COLAGG generally produces more scattering compared to the COL and COLHOMO cases for bands 5 and 6, and significantly more than COL80 and COL120. The larger generalized effective size of COL80 and COL120 produces progressively larger absorption, as expected.

The bottom row shows the leading Legendre expansion coefficient of the phase function, $\omega_1/3$, which is equal to the asymmetry factor. The asymmetry factor describes the amount of radiation that is scattered in the projected forward direction minus the scattering projected in the backward direction. The plots indicate that there is slightly greater forward scattering from the COL compared to the COLAGG case. The aggregates have more scattering backwards than columns due to the multifaceted shape.

5. Numerical sensitivities of ice crystal properties of cirrus

We now use the optics derived above for the EMERALD1 EM09 case as well as cases with assumptions of generalized effective size in order to evaluate radiative properties such as upwelling flux at the top of the model atmosphere and downwelling flux evaluated at the surface, in order to assess the impact of making various assumptions regarding vertical structure, habit and size distribution. The seven cases described in section 4.1 have been implemented in the LEM and the results were assessed in terms of the radiative properties and effects on cirrus cloud evolution. To contrast the results, we have included a section looking at the sensitivity of the results to ice particle roughness. The low value of the asymmetry parameter for rough particles is believed to have significant effects on the magnitude of cirrus cloud radiative properties (Ulanowski *et al.*, 2006) and will offer an interesting comparison.

5.1. Effect of vertical structure, habit and size on radiative properties of cirrus

In this section, we focus on understanding the effects of vertical structure, habit and size distributions on radiative properties. We focus on three ways of targeting effects. The first targets assumptions about the vertical profile of ice particles (i.e. size distributions), the second targets the vertical variation of ice particle habits and the third targets the effect of not making use of the observed vertical structure (averaged vertical profiles or ignoring EMERALD1 observations altogether). For all of these, the effects are assessed quantitatively by evaluating the radiative properties.

As stated, the most accurate treatment is case 1: COLAGG. In Figure 6 we see the difference plot of COLAGG–COL, which isolates the effect of explicit treatment of rosettes and

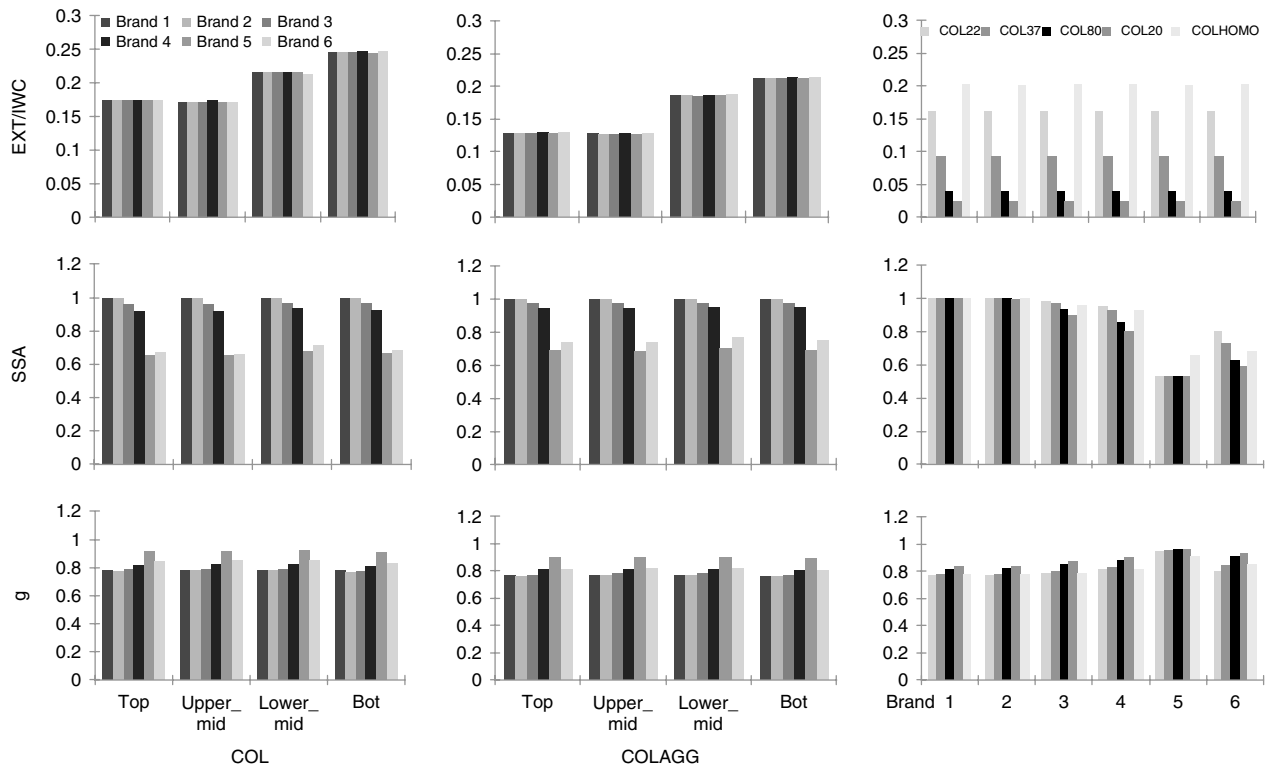


Figure 5. The plots in the top row are for extinction coefficient per unit IWC; the middle row is SSA; the bottom row is asymmetry factor (g). The first two columns are for column-only and for column and aggregate. The optical properties are calculated from *in situ* size distributions and habit information from EM09 and the optics from Baran compilation. The vertical structures of habit in the cloud for EM09 is specified as ‘Top’, ‘Upper_mid’, ‘Lower_mid’ and ‘Bot’, and indicate the location within the cloud in the vertical. The last column includes four runs using the Fu–Liou radiation scheme with fixed r_e of 20, 37, 80 and 120 μm . COLHOMO means the vertical structure has been averaged.

aggregates (as opposed to as columns). This effect results in a difference in the downward flux at the surface of approximately 16 W m^{-2} and over 10 W m^{-2} difference in the upward flux at the top of the model atmosphere.

By homogenizing to obtain the column-only case (COLHOMO) we remove not only variations in habits but also all vertical variations. In Figure 6 we note that homogenizing the layer acts in opposition to the effects of just changing the habit from COLAGG to COL. The downward flux difference at the surface is now about 8 W m^{-2} and a 2 W m^{-2} difference in the upward flux at the top of the model.

Figure 7 shows the difference between COLAGG and three assumed constant generalized effective sizes (standard in the Fu–Liou scheme) which span the full range of typical sizes from observations (Fu, 1996): 20, 80 and 120 μm . For comparison, the value of 37.4 μm (labelled COL37) is also used (the value derived from the observed size distributions). By comparing these commonly assumed generalized effective size with our most accurate treatment, COLAGG, we find that differences in upward and downward fluxes in excess of 100 W m^{-2} are frequent. This illustrates the importance of using accurate values of effective size and the errors that can occur if commonly used values (over observed ranges) are assumed. Also, the difference between COL and COL37 shows that the fluxes are sensitive to either the optics used or differences in the observed and assumed size distributions underlying the calculations.

Difference in downward and upward solar radiative flux at time 120 min (left) and 165 min (right) for EMERALD1-specific optical properties compared to Fu–Liou assumed generalized effective sizes.

5.2. Effect of roughness on radiation

Roughness of ice particles is anticipated to be a very important yet uncertain factor for ice cloud radiative properties (Ulanowski *et al.*, 2006; Yang *et al.*, 2008; Ulanowski *et al.*, 2010). [Correction added on 22 December 2011 after original online publication: in the preceding sentence the text ‘a very important factor and is currently neglected in ice cloud radiative properties’ has been replaced.] Although the degree and frequency of occurrence of roughness in cirrus are largely unknown, and we are unaware if it occurred in the EMERALD1 case, it is instructive to compare the effects of the last section to those of roughness. Currently, roughness is believed mostly to affect the asymmetry factor, and typical values of non-rough asymmetries in cirrus vary from 0.7 (Stephens *et al.*, 1990), to 0.75 (Garrett *et al.*, 2001), to 0.8 (Francis *et al.*, 1994) and more than 0.85 (Fu, 2007). Our base case of COL37 has an asymmetry of 0.78 for a generalized effective size of 37.4 μm (Fu, 1996).

In Figure 8, we illustrate the effects of rough particles. We have performed runs using asymmetry values that range from non-rough (COL37) through to progressively rougher particles with an asymmetry of 0.65 (labelled COL37(65)) (Ulanowski *et al.*, 2006). At the lowest value of asymmetry equal to 0.65, we see that upward and downward fluxes can differ by over 25 W m^{-2} relative to the COL37 case with no roughness. This is more than triple the effect of vertical structure; however, for more conservative changes to asymmetry, say between COL(70) and COL(75), the effect of roughness is about $10\text{--}15 \text{ W m}^{-2}$. This is similar

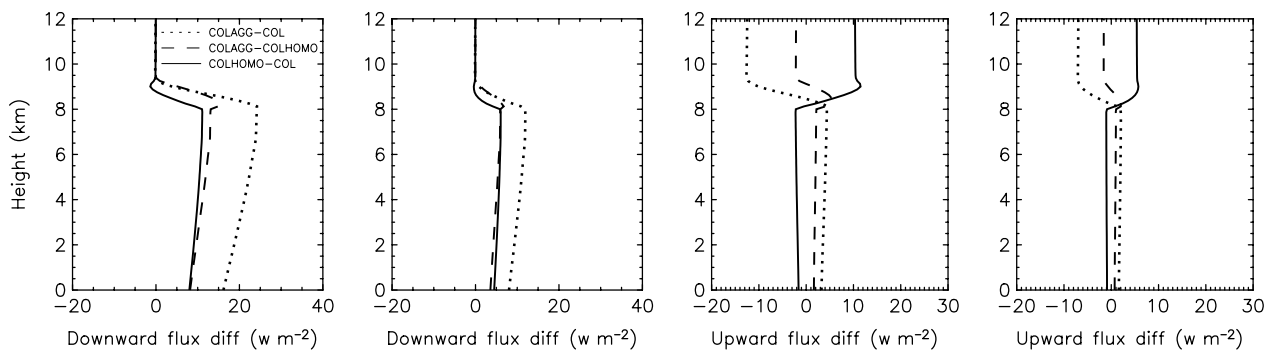


Figure 6. Difference in the solar fluxes for EMERALD1-specific optical properties with habit variations (COLAGG and COL) and vertical homogenizing (COLHOMO). The difference in downward solar flux at 120 and 165 min are shown in the first two plots on the left-hand side, respectively. The difference in upward solar flux at 120 and 165 min are shown in the remaining two plots, respectively.

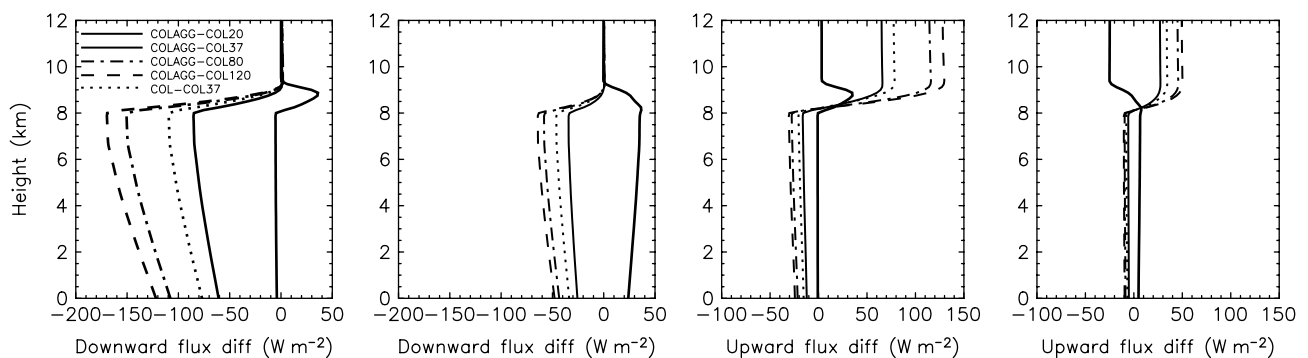


Figure 7. Difference in the solar fluxes for EMERALD1-specific optical properties compared to Fu-Liou assumed generalized effective sizes. The difference in downward solar flux at 120 and 165 min are shown in the first two plots on the left-hand side, respectively. The difference in upward solar flux at 120 and 165 min are shown in the remaining two plots, respectively.

in magnitude to the effect of vertical structure and habit effects.

5.3. Effect of vertical structure on cirrus cloud evolution and lifetime

Shown in Figure 9 are IWPs with time plots for the seven base cases over the 4 h simulation period. It is clear that there is little variation in the IWP with time for six out of the seven cases. The smallest generalized effective size case of 20 μm (case 4, COL20), however, illustrates a significantly different behaviour, with the IWP remaining much higher than the other cases for significantly longer, especially during the decay period of the cloud over the last 2 h. At the end of the simulation period, the COL20 case has an order of magnitude higher IWP.

By comparing the average radiative properties over the duration of the simulation, we find that the COL20 case leads to a higher average upward solar flux at the top of the atmosphere of 42 W m^{-2} and reduced average downward flux of 39 W m^{-2} compared with the COL37 case. We compared to the COL37 case rather than COLAGG so as to isolate only the effects of evolution without introducing other changes.

6. Conclusions

This work presents an analysis of the importance of vertical structure of habits and size distributions on the radiative properties based on observations of the EMERALD1 campaign. The EMERALD1 campaign was selected since one of the runs, EM09, had flight paths designed to assess

the vertical structure of the cloud, and ice crystal habit and size distribution had been analysed and were available for this study. In addition to the vertical structure of habit and size distribution, an assessment was carried out illustrating the effects of making progressively more simplistic assumptions regarding habit and size distribution, beginning with using the full EMERALD1 observed ice properties through to using typical literature values and no EMERALD1 observations. This was designed to show modellers the relative importance of making each step up or down in complexity. The study overall focused on seven modelled cases which targeted various aspects of habit, size distribution and vertical variation effects, as well as various simplifications. The effects of these properties were quantitatively evaluated in terms of impact on radiative properties and evolution of the modelled cirrus cloud. The modelling was performed with UK Met Office LEM with EMERALD1 specific optical properties installed.

The importance of vertical structure observed from the EMERALD1 observations was evaluated by comparing cases with and without vertical structure and it was found that there was a change in the upward and downward solar fluxes at the top and surface of the model atmosphere of 8 and 10 W m^{-2} , respectively.

An assessment was then performed to determine the importance of including information about habit beyond columns in the optics calculations. By comparing the modelled cases in which all habits are treated optically as columns compared to that in which aggregates and rosettes are treated as aggregate habits in the optics, we found this leads to a 12 W m^{-2} change in the upward and a 16 W m^{-2} change in the downward fluxes.

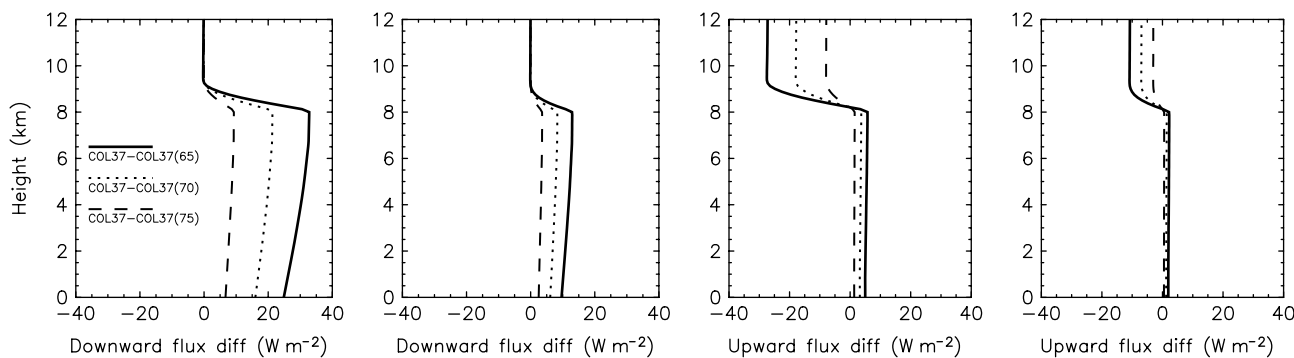


Figure 8. Difference in the downward and upward solar radiative flux for rough particles for the case of generalized effective size of $37\ \mu\text{m}$ shown for times 120 and 165 min. COL37(65), COL37(70), COL37(75), and COL37 indicate the asymmetry values representing a progression from rough to smooth crystals.

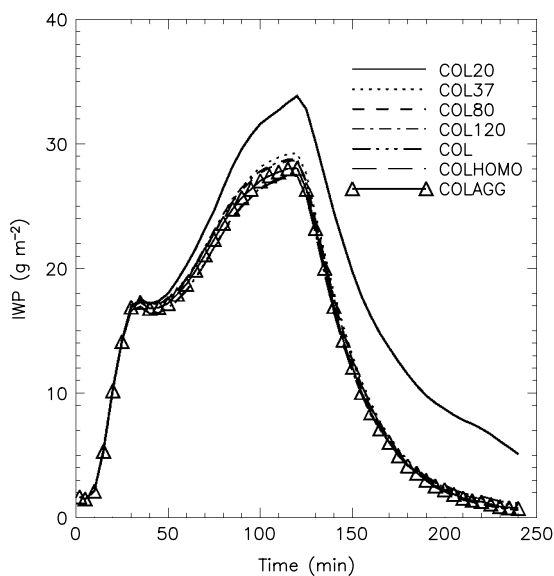


Figure 9. Ice water path time evolution.

Both of these effects summarized above are significant and should not be considered in isolation. For example, by comparing the most complex habit optics treatment (COLAGG) with the vertically homogenized column (COLHOMO) results it was found that the difference in fluxes was $2\ \text{W m}^{-2}$ for the upward and $8\ \text{W m}^{-2}$ for the downward fluxes. Thus it was noted that vertical structure and habit specification were found to counteract one another in terms of radiative properties. Therefore modellers seeking to step up the treatment of complexity in their models by only one of these factors—either more complex habits or size distribution vertical structure—can experience worse agreement than by not including both competing factors together.

The choice of effective size (and habit complexity) in models is often parametrized and usually very simplistic or even fixed. Models are unlikely to capture the actual evolution of effective size, especially if fixed values are used. In this work, we knew the actual generalized effective size from the EMERALD1 observations, but in a model run we would not know this value and so a range of values was used from the literature to illustrate the potential range of error in fluxes that might result. We used an observed range in generalized effective size ($20\text{--}120\ \mu\text{m}$) for the comparison. We found that errors spanned up to and

exceeding $100\ \text{W m}^{-2}$ for both the upward and downward fluxes compared to our most detailed optics treatment of COLAGG and knowledge of the observed sizes and habits. Inaccurate specification of the effective size produced the largest differences in the study for the instantaneous radiative fluxes.

LEM simulations were used to evaluate the importance of vertical structure and size distribution on the modelled cloud evolution. The results showed no significant effect on cloud evolution for the EMERALD1 case. Past results have shown significant effects when switching the whole cloud between habits (Liu *et al.*, 2003); however, for this EMERALD1-based case with observed habit size distributions the effect was small. A strong sensitivity in the cloud lifetime, however, was noted for a small generalized effective size of $20\ \mu\text{m}$ (case COL20). The effect on lifetime was very significant, leading to a factor of ten greater IWP at the end of the simulation compared to the other cases. This suggests that simulations using a generalized effective size roughly $30\ \mu\text{m}$ or greater for a cloud that in reality had a smaller generalized effective size could lead to a very significant underestimate of the cloud lifetime (about $40\ \text{W m}^{-2}$ averaged over the simulation duration), although this has to be tempered with the fact that solar radiative heating effects may be less influential in small effective size cases due to the often coincident smaller observed ice water contents (Fu, 1996).

To add further perspective to the results above, we have estimated the importance of roughness for our study, since roughness is currently considered a potentially very important yet highly uncertain effect. Roughness was simulated by reducing the asymmetry factor progressively down to a value of 0.65 (rough). For an asymmetry of 0.65, the radiative properties were changed by over $25\ \text{W m}^{-2}$ both for upward flux at the top of the atmosphere and downward flux at the surface relative to the non-rough case. The effect of roughness is poorly understood and our result is at best an estimate. Given the uncertainty, if a moderate value of roughness is used, say between 0.70 and 0.75, then the effect on radiative fluxes is roughly $10\text{--}15\ \text{W m}^{-2}$, which is similar in magnitude to the effects of ice particle habits and vertical structure illustrated in this work.

Acknowledgements

We are grateful to Dr Anthony Baran (UK Met Office) for providing the optical property database used in this study. We would like to acknowledge the UK National Environment Research Council (NERC) Facility for Ground

Based Atmospheric Measurement (FGAM) for providing the CPI data. We would also like to acknowledge the UK Met Office for the provision of the Large Eddy Model (LEM).

References

- Auer AH, Veal DL. 1970. The dimension of ice crystals in natural cloud. *J. Atmos. Sci.* **61**: 514–544.
- Baran AJ. 2009. A review of the light scattering properties of cirrus. *J. Quant. Spectrosc. Radiat. Transfer* **110**: 1239–1260.
- Baran JA, Labonnote LC. 2007. A self-consistent scattering model for cirrus. I: The solar region. *Q. J. R. Meteorol. Soc.* **133**: 1899–1912.
- Baran AJ, Francis PN, Labonnote LC, Doutriaux-Boucher M. 2001. A scattering phase function for ice cloud: tests of applicability using aircraft and satellite multi-angle multi-wavelength radiance measurements of cirrus. *Q. J. R. Meteorol. Soc.* **127**: 2395–2416.
- Baran AJ, Francis PN. 2004. On the radiative properties of cirrus cloud at solar and thermal wavelengths: A test of model consistency using high-resolution airborne radiance measurements. *Q. J. R. Meteorol. Soc.* **130**: 763–778.
- Chou MD, Lindzen RS, Hou AY. 2002. Reply to: 'Tropical cirrus and water vapor: an effective earth infrared iris feedback?' *Atmos. Chem. Phys.* **2**: 173–180.
- Connolly PJ, Flynn MJ, Ulanowski Z, Choullarton TW, Gallagher MW, Bower KN. 2007. Calibration of 2-D imaging probes using calibration beads and ice crystal analogues: the depth of field. *J. Atmos. Ocean. Technol.* **24**: 1860–1879.
- Dobbie S, Jonas P. 2001. Radiative influences on the structure and lifetime of cirrus clouds. *Q. J. R. Meteorol. Soc.* **127**: 2263–2682.
- Dobbie S, Li J, Chylek P. 1999. Two- and four-stream optical properties for water clouds and solar wavelengths. *J. Geophys. Res.* **104**: 2067–2079.
- Dowling DR, Radke LF. 1990. A summary of the physical properties of cirrus clouds. *J. Appl. Meteorol.* **29**: 970–978.
- Ebert EE, Curry JA. 1992. A parameterization of cirrus cloud optical properties for climate models. *J. Geophys. Res.* **97**: 3831–3836.
- Edwards JM, Havemann S, Thelen JC, Baran AJ. 2007. A new parameterization for the radiative properties of ice crystals: comparison with existing schemes and impact in a GCM. *Atmos. Res.* **83**: 19–34.
- Field PR, Heymsfield AJ. 2003. Aggregation and scaling of ice crystal size distributions. *Q. J. R. Meteorol. Soc.* **122**: 689–719.
- Francis PN, Jones A, Saunders RW, Shine KP, Slingo A, Sun Z. 1994. An observational and theoretical study of the radiative properties of cirrus: some results from ICE89. *Q. J. R. Meteorol. Soc.* **120**: 809–848.
- Fu Q. 1996. An accurate parameterization of the solar radiative properties of cirrus clouds for climate models. *J. Climate* **9**: 2058–2082.
- Fu Q. 2007. A new parameterization of an asymmetry factor of cirrus clouds for climate models. *J. Atmos. Sci.* **64**: 4140–4150.
- Fu Q, Liou KN. 1992. On the correlated k-distribution method for radiative transfer in nonhomogeneous atmosphere. *J. Atmos. Sci.* **49**: 2139–2156.
- Fu Q, Liou KN. 1993. Parameterization of the radiative properties of cirrus clouds. *J. Atmos. Sci.* **50**: 2008–2025.
- Fu Q, Yang P, Sun WB. 1998. An accurate parameterization of the infrared radiative properties of cirrus clouds for climate models. *J. Climate* **11**: 2223–2237.
- Fu Q, Baker M, Hartmann D. 2002. Tropical cirrus and water vapour: an effective earth infrared iris feedback? *Atmos. Chem. Phys.* **2**: 31–37.
- Gallagher MW, Connolly PJ, Whiteway J, Figueras-Nieto D, Flynn M, Choullarton TW, Bower KN, Cook C, Busen R, Hacker J. 2005. An overview of the microphysical structure of cirrus clouds observed during EMERALD-1. *Q. J. R. Meteorol. Soc.* **131**: 1143–1169.
- Garrett TJ, Hobbs PV, Gerber H. 2001. Shortwave, single-scattering properties of arctic ice clouds. *J. Geophys. Res.* **106**: 15155–15172.
- Gray MEB, Petch J, Derbyshire SH, Brown AR, Lock AP, Swann HA. 2001. *Version 2.3 of the Met Office Large Eddy Model*. Met Office, Exeter, UK.
- Gu Y, Liou KN. 2004. Cirrus cloud horizontal and vertical inhomogeneity effects in a GCM. *Meteorol. Atmos. Phys.* **91**: 223–235.
- Heymsfield AJ, McFarquhar GM. 2002. Mid latitude and tropical cirrus. In *Cirrus*, Lynch DK, Sassen K, Starr DO'C, Stephens G (eds). Oxford University Press: Oxford; 78–101.
- Heymsfield AJ, Miller KM. 1990. The 27–28 October 1986 FIRE IFO cirrus case study: cloud microstructure. *Mon. Weather Rev.* **118**: 2313–2328.
- Heymsfield AJ, Platt CMR. 1984. A parameterization of the particle spectrum of ice clouds in terms of the ambient temperature and the ice water content. *J. Atmos. Sci.* **41**: 846–855.
- Kahnert M, Nousiainen T, Raisanen P. 2007. Mie simulations as an error source in mineral aerosol radiative forcing calculations. *Q. J. R. Meteorol. Soc.* **133**: 299–307.
- Key JR, Yang P, Baum BA, Nasiri SL. 2002. Parameterization of shortwave ice cloud optical properties for various particle habits. *J. Geophys. Res.* **107**: 4181, DOI: 10.1029/2001JD000742.
- Lemke H, Quante M, Danne O, Raschke E. 1999. The role of ice particle shape and size distributions in polarimetric radar measurements at 95 GHz. *Proceedings, IEEE IGARSS '99*; 149–151.
- Li J, Dobbie JS. 1997. Four-stream isosector approximation for solar radiative transfer. *J. Atmos. Sci.* **55**: 558–567.
- Lin B, Wielicki BA, Chambers LH, Hu Y, Xu KM. 2002. The iris hypothesis: a negative or positive cloud effect? *J. Climate* **15**: 3–7.
- Lindzen RS, Chou MD, Hou AY. 2001. Does the earth have an adaptive infrared iris? *Bull. Am. Meteorol. Soc.* **82**: 417–432.
- Liou KN. 1986. Influence of cirrus clouds on weather and climate processes: a global perspective. *Mon. Weather Rev.* **114**: 1167–1199.
- Liou KN. 2002. *An Introduction to Atmospheric Radiation* (2nd edn). Academic Press: London.
- Liu KN, Wang PK, Schlesinger RE. 2003. A numerical study of cirrus clouds. Part II: Effects of ambient temperature, stability, radiation, ice microphysics, and microdynamics on cirrus evolution. *J. Atmos. Sci.* **60**: 1097–1119.
- Macke A. 1993. Scattering of light by polyhedral ice crystals. *Appl. Optics* **32**: 2780–2788.
- Marshall JH, Dobbie S. 2005. The effects of wind shear on cirrus: a large-eddy model and radar case-study. *Q. J. R. Meteorol. Soc.* **131**: 2937–2955.
- Marshall JH, Dobbie S, Hogan RJ. 2006. Evaluation of a large-eddy model simulation of a mixed-phase altocumulus cloud using microwave radiometer, lidar and doppler radar data. *Q. J. R. Meteorol. Soc.* **132**: 1693–1715.
- Mason PJ. 1989. Large-eddy simulation of the convective atmospheric boundary layer. *J. Atmos. Sci.* **46**: 1492–1516.
- McFarquhar GM, Heymsfield AJ. 1996. Microphysical characteristics of three anvils sampled during the Central Equatorial Pacific Experiment (CEPEX). *J. Atmos. Sci.* **53**: 2401–2423.
- McFarquhar GM, Yang P, Macke A, Baran AJ. 2002. A new parameterization of single scattering solar radiative properties for tropical anvils using observed ice crystal size and shape distributions. *J. Atmos. Sci.* **59**: 2458–2478.
- Mitchell DL, Arnott WP. 1994. Model predicting the evolution of ice particle spectra and radiative properties of cirrus cloud. II. Dependence of absorption and extinction on ice crystal morphology. *J. Atmos. Sci.* **51**: 817–832.
- Stephens GL, Tsay SC, Stackhouse PW, Flatau PJ. 1990. The relevance of the microphysical and radiative properties of cirrus clouds to climate and climate feedback. *J. Atmos. Sci.* **47**: 1742–1753.
- Stubenrauch CJ, Eddouina F, Edwards JM, Macke A. 2007. Evaluation of cirrus parameterizations for radiative flux computations in climate models using TOVS-ScaRaB satellite observations. *J. Climate* **20**: 4459–4475.
- Takano Y, Liou KN. 1989. Solar radiative transfer in cirrus clouds. Part I: Single-scattering and optical properties of hexagonal ice crystals. *J. Atmos. Sci.* **46**: 3–19.
- Takano Y, Liou KN. 1995. Radiative transfer in cirrus clouds. Part III: Light scattering by irregular ice crystals. *J. Atmos. Sci.* **52**: 818–837.
- Thekaekara MP. 1973. Solar energy outside the earth's atmosphere. *Sol. Energy* **14**: 109–127.
- Ulanowski Z, Hesse E, Kaye PH, Baran AJ. 2006. Light scattering by complex ice-analogue crystals. *J. Quant. Spectrosc. Radiat. Transfer* **100**: 382–392.
- Ulanowski Z, Kaye PH, Hirst E, Greenaway RS. 2010. 'Light scattering by ice particles in the Earth's atmosphere and related laboratory measurements'. In *Electromagnetic and Light Scattering XII Conference*, Finland.
- Um J, McFarquhar G. 2009. *Single-scattering Properties of Aggregates of Plates*. *Q. J. R. Meteorol. Soc.* **135**: 291–304.
- Wang PH, McCormick MP, Minnis P, Kent GS, Skeens KM. 1996. A 6-year climatology of cloud occurrence frequency from SAGE II observations (1985–1990). *J. Geophys. Res.* **101**: 29407–29429.
- Wang Z, Sassen K. 2001. Cirrus cloud microphysical property retrieval using lidar and radar measurements. Part I: Algorithm description and comparison with in situ data. *J. Appl. Meteorol.* **41**: 218–229.
- Whiteway J, Cook C, Gallagher M, Choullarton T, Harries J, Connolly P, Busen R, Bower K, Flynn M, May P, Aspey R, Hacker J. 2004. Anatomy of cirrus clouds: results from the Emerald airborne campaigns. *Geophys. Res. Lett.* **31**: L24102, DOI: 10.1029/2004GL021201.
- Wylie DP, Menzel WP. 1999. Eight years of high cloud statistics using HIRS. *J. Climate* **12**: 170–183.

- Wylie DP, Menzel WP, Strabala KI. 1994. Four years of global cirrus cloud statistics using HIRS. *J. Climate* **7**: 1972–1986.
- Yang H. 2009. 'The GCSS ARM SGP March 9, 2000 cirrus cloud case study and inter-comparison: development and first results including selected cloud-scale sensitivities'. PhD thesis, University of Leeds.
- Yang P, Liou KN, Wyser K, Mitchell D. 2000. Parameterization of the scattering and absorption properties of individual ice crystals. *J. Geophys. Res.* **105**: 4699–4718.
- Yang P, Gao B-C, Baum BA, Wiscombe W, Hu YX, Nasiri SL, Soulen PF, Heymsfield A, McFarquhar GM, Miloshevich L. 2001. Sensitivity of cirrus bidirectional reflectance to vertical inhomogeneity of ice crystal habits and size distributions for two moderate-resolution imaging spectroradiometer (MODIS) bands. *J. Geophys. Res.* **106**: 17267–17291.
- Yang P, Kattawar WK, Hong G, Minnis P, Hu YX. 2008. Uncertainties associated with the surface texture of ice particles in satellite-based retrieval of cirrus clouds. Part I: Single-scattering properties of ice crystals with surface roughness. *IEEE Trans. Geosci. Remote Sens.* **46**: 1940–1947.
- Zhang Y, Mace GG. 2006. Retrieval of cirrus microphysical properties with a suite of algorithms for airborne and spaceborne lidar, radar, and radiometer data. *J. Appl. Meteorol. Climatol.* **45**: 1665–1689. [Correction added on 22 December 2011 after original online publication: references for Baran *et al.*, 2000, Havemann and Baran, 2001, Havemann *et al.*, 2002, and Yang *et al.*, 2005, were removed from the reference list since a post-publication correction meant that they were no longer cited in the text, and the reference for Baran and Francis, 2004, was added.]